

# An Overview of the Basic Physical Properties of $\text{MgB}_2$

P.C. Canfield,\* S.L. Bud'ko, D.K. Finnemore

*Ames Laboratory and Department of Physics and Astronomy, Iowa State  
University, Ames, IA 50011, USA*

---

## Abstract

The basic physical properties of  $\text{MgB}_2$  have been well established over the past two years of intensive research. At this point there is a general consensus about the values for the isotope shift, critical fields, most of the salient length scales, and general anisotropies. In this paper we will review the determination of these parameters and set the stage for further, more detailed discussions of specific aspects of the physics of  $\text{MgB}_2$ .

---

## 1 Introduction

Given that the existence of superconductivity in  $\text{MgB}_2$  was only announced in January of 2001, [1] there has been an explosive growth in humanity's understanding of the basic physical properties of this simple binary compound over the past two years. At this point in time there is a consensus about most of the fundamental properties of this material and a rapidly growing understanding of, as well as appreciation for, the dramatic differences between this extreme example of BCS superconductivity and other, older examples of intermetallic superconductivity.

In this paper we will summarize the status of our experimental understanding of the basic properties associated with the normal and superconducting states of  $\text{MgB}_2$ .

---

\* Corresponding author.

*Email address:* canfield@ameslab.gov (P.C. Canfield,).

## 2 Experimental procedures

All of the data presented in this paper comes from measurements of polycrystalline samples of  $\text{MgB}_2$ . Two basic types of samples were used: sintered pellets and wire segments. Both types of samples were synthesized by exposing boron to Mg vapor at, or near,  $950^\circ\text{C}$ . The sintered pellets were made by combining stoichiometric amounts of high purity magnesium and isotopically pure boron and reacting them in a sealed Ta tube. [2,3] The wire segments were made by using a different initial form of boron: boron filament. In this case the boron filament was exposed to magnesium vapor by sealing it in a Ta tube with excess Mg and heating to or near  $950^\circ\text{C}$ . [4] This same method has been used to transform thin films of boron into  $\text{MgB}_2$  thin films. [5] As those skilled in the art will realize, the steps outlined above provide a form preserving method of turning boron objects (filaments, films, tapes) into  $\text{MgB}_2$  objects with similar morphologies. [6] Polycrystalline  $\text{MgB}_2$  synthesized in this manner is single-phased and, as will be discussed below, manifests the properties of a high purity sample. Further details about sample synthesis can be found in references [2,3,4,5,6] as well as the paper by Ribeiro *et al.* in this volume.

Virtually all the measurements presented in this paper were performed on Quantum Design MPMS-5, MPMS-7, and PPMS-9 machines. Electrical contact was made to the samples by using Epotek H20E silver epoxy and Pt wires. High field magneto-transport data was measured at the National High Magnetic Field Laboratory in Los Alamos for magnetic field up to 18 T. [7]

## 3 Isotope effect measurements

Immediately after the announcement of the discovery of superconductivity in  $\text{MgB}_2$  the first question that had to be addressed was one of mechanism. Whereas most researchers experienced with intermetallic compounds assumed that  $\text{MgB}_2$  was the long sought after, extreme example of phonon-mediated, BCS superconductivity, some researchers, steeped in the lore of high- $T_c$  oxides, assumed that a 40 K superconductor had to stem from a more exotic coupling mechanism. The simplest way to shed light on this question was to measure the boron isotope shift of  $T_c$ . Looking at boron rather than magnesium was motivated by physical, economic and time considerations. Given the high  $T_c$  of  $\sim 40$  K it seemed likely that the lightest (as well as most prevalent) element would be responsible for the phonons associated with the pairing of electrons. In addition, isotopically pure boron is relatively cheap given its natural abundance ( $\sim 80\%$   $^{11}\text{B}$  and  $20\%$   $^{10}\text{B}$ ) and the fact that its light atomic weight allow for separation via diffusion rather than requiring mass spectroscopy. This fact

means that many materials preparation labs, particularly ones working with neutron scatters (who require the use on non-absorbing  $^{11}\text{B}$ ), have supplies of isotopically pure boron on hand.

Figure 1 presents temperature dependent electrical resistance and magnetization data taken on  $\text{Mg}^{11}\text{B}_2$  and  $\text{Mg}^{10}\text{B}_2$  samples. A clear 1.0 K shift in  $T_c$  can be seen in both measurements. Specific heat data (not shown) taken on the same samples show the same 1.0 K shift.[2] This 1.0 K shift is to be compared with the simple prediction of the BCS model,  $\Delta T_c \sim 0.85$  K, based upon  $T_c \propto 1/(\text{formula unit mass})^{-1/2}$ . The partial isotope exponent for boron is  $\alpha_B = 0.26$ . [2]. These data by themselves are not proof that Cooper pair formation in  $\text{MgB}_2$  is mediated by phonons, but it is consistent with it and strongly reinforced the idea that  $\text{MgB}_2$  was an extreme example of phonon-mediated BCS superconductivity.

Subsequent measurements [8] confirmed the boron isotope shift and found that there was virtually no magnesium isotope shift. All of the isotope shift data have subsequently explained within the context of phonon-mediated, BCS superconductivity. [9,10,11].

#### 4 Basic properties

Once the question of mechanism has been addressed, the next set of questions that arise concern the basic properties associated with both the normal and superconducting state. Let's start with electrical transport. Figure 2 (upper panel) presents the temperature dependent resistance of a piece of sintered pellet for various values of applied magnetic field. Given that the density of the sintered pellet is not close to 100% we can only estimate the resistivity of  $\text{MgB}_2$  at 42 K to be  $\sim 1 \mu\Omega\text{-cm}$  based on these data. On the other hand what can be clearly seen is that there is a substantial loss of scattering associated with cooling the sample from 300 K down to 40 K. In fact the residual resistivity ratio ( $RRR$ ),  $R(300 \text{ K})/R(42 \text{ K})$ , is close to 20. A consequence of this very low, normal state resistance is the substantial magneto-resistance observed in the normal state. These effects can be seen even more clearly in the temperature dependent resistivity data from the  $\text{MgB}_2$  wire segment (Fig. 2, lower panel). Given a sample density of better than 95% combined with a well-defined geometry the resistivity can be easily determined: e.g.  $\rho(300 \text{ K}) = 9.6 \mu\Omega\text{-cm}$  and  $\rho(40 \text{ K}) = 0.38 \mu\Omega\text{-cm}$ . The temperature dependence of the wire sample is quantitatively similar to that seen for the sintered pellet and it manifests the same, large, normal-state magneto-resistivity.

The value of the low temperature, normal-state resistivity is important for two rather different reasons. If we take  $v_F = 4.8 \times 10^7$  cm/s we can extract

an electronic mean free path of  $l \sim 600 \text{ \AA}$ . [4] As will be shown below, when this length scale is compared to the superconducting coherence length,  $\xi_0$ , it becomes clear that  $\text{MgB}_2$  is deep in the clean limit of superconductivity, i.e.  $l \gg \xi_0$ . A low resistivity is also very important for possible applications, specifically high current ones. An intrinsically small, low-temperature, normal state resistivity means that there is far less chance of quenching magnets made from this material.

Figure 3 presents the normal state magneto-transport data, shown in part in the lower panel of Fig. 2 as well as the inset of Fig. 3, in the form of a Kohler plot. [7,12] The fact that all of these data fall onto a single manifold is consistent with  $\text{MgB}_2$  being a simple ( $s$ - and  $p$ -band) metal with a single salient scattering time in the normal state. These data, along with the isotope effect data, help demonstrate that  $\text{MgB}_2$  is indeed a representative example of intermetallic superconductivity, i.e. there is no need for more exotic, high- $T_c$ -like, theoretical explanations.

It should be noted though, that whereas we have had no difficulty in preparing high-purity, low resistivity, polycrystalline samples of  $\text{MgB}_2$ , other groups had difficulty in reproducing these results. Residual resistivity values as high as  $70 \mu\Omega\text{-cm}$  [1] or  $20 \mu\Omega\text{-cm}$  [13] have been reported. In addition it was suggested that metallic magnesium in parallel with the  $\text{MgB}_2$  could be responsible for the low resistivities we have found. [14,15] This controversy spurred us to examine the possible sources of this apparent variation in sample quality (see reference [3] as well as paper by R. Ribeiro *et al.* in this volume). We found that the use of very high purity boron is vital to the formation of low resistivity samples. We also found that for the stoichiometric pellets as well as the wire segments formed via exposure to boron filament to Mg vapor the low resistivity is not associated with free magnesium, but rather is an intrinsic feature of high purity  $\text{MgB}_2$ . Fortunately as more and more data on  $\text{MgB}_2$  (polycrystals, films, and single crystals) becomes available there values of both room temperature and residual resistivity are asymptotically approaching the values presented in Fig. 2. [16,17,18]

The magneto-transport data shown in Fig. 2 can also be used to extract information about the superconducting state, specifically the upper critical field,  $H_{c2}(T)$ . The  $H_{c2}(T)$  data are plotted in Fig. 4.  $H_{c2}(T)$  rises to slightly above 16 T at 1.5 K. [7] From this value we can extract an estimate of  $\xi_0$  of  $\sim 50 \text{ \AA}$ , a value that is indeed much less than the electronic mean free path,  $l \sim 600 \text{ \AA}$ . As mentioned above, given that  $l \gg \xi_0$ ,  $\text{MgB}_2$  is deep within the clean limit of superconductivity.

There are several other field scales of interest: the irreversibility field,  $H_{irr}$  and the thermodynamic critical field,  $H_c$ . Figure 5 presents  $M(H)$  data that clearly show the irreversibility field for representative temperatures. The  $H_{irr}(T)$

curve deduced from these data is presented as the lower curve in Fig. 4. As can be seen,  $H_{irr}$  is approximately one half of  $H_{c2}$ . Whereas the values of  $H_{c2}(1.5 \text{ K}) \sim 16 \text{ T}$  and  $H_{irr}(5 \text{ K}) \sim 7 \text{ T}$  are neither very low nor very high, there are already examples of dirtier samples for which the low temperature  $H_{c2} \sim 30 \text{ T}$  and the low temperature  $H_{irr} \sim 15 \text{ T}$ . [19,20] One of the current, key areas of applied research on MgB<sub>2</sub> is focusing on the attempt to understand how pinning, as well as  $\kappa$ , in this material can be simply and reproducibly controlled.

The thermodynamic critical field can be inferred, at least for  $T$  near  $T_c$ , from magnetization loops. [12] The inset to Fig. 6 presents  $H_c(T)$  for  $T$  close to  $T_c$ .  $H_c(T)$  was determined by integrating the area under the equilibrium magnetization versus field curve where  $M_{eq} = (M_{inc} + M_{dec})/2$ , and  $M_{inc}$  and  $M_{dec}$  are the increasing field magnetization and decreasing field magnetization respectively. [12] The  $H_c(T)$  data can be used to estimate another length scale, the London penetration depth,  $\lambda$ , by using the simple relations  $\kappa = H_{c2}/[1.41H_c] = \lambda/\xi_0$ . Using the  $H_{c2}(T)$  data from Fig. 4 as well as the  $H_c(T)$  data from Fig. 6 we find that  $\kappa \sim 25$  and  $\lambda \sim 1400 \text{ \AA}$ .

The values of  $l$ ,  $\xi_0$ ,  $\lambda$  and  $\kappa$  derived above are average values. There has been no effort made to account for the anisotropy associated with the hexagonal unit cell of MgB<sub>2</sub>. This means that these values should be taken as bench marks rather than definitive, final values. The reason for this caveat is the fact that there are very large anisotropies in many of the properties of MgB<sub>2</sub>. Perhaps the most conspicuous is the anisotropy in the value of  $H_{c2}(T)$ . [21,22,23,24] Whereas early estimates of this anisotropy,  $\gamma \equiv H_{c2}^{basal \ plane}/H_{c2}^{c-axis}$ , were rather low ( $\gamma = 1.73$ ), [21] measurements on unoriented, high purity powders allowed us to determine the anisotropic  $H_{c2}(T)$  in detail. [23,24] Figure 7 presents the temperature dependence of the anisotropic  $H_{c2}(T)$  curves. The lower curve is for the crystallites with the field aligned along the crystallographic  $c$ -axis and the upper curve is for the crystallites with the field aligned along the basal plane. [21,22] At low temperatures  $\gamma$  approaches a remarkably high value between 6 and 7. Over the past several months, detailed measurements on small single crystalline samples have confirmed not only the size of the low temperature anisotropy, but also the full temperature dependence of  $\gamma(T)$ . [25,26] The low temperature value of the anisotropy,  $\gamma = 6-7$ , is in excellent agreement with the anisotropic  $H_{c2}(T)$  that would be anticipated if only the two dimensional, cylindrical Fermi surface is responsible for the low- $T$ ,  $H \geq 2 \text{ T}$ , superconductivity. [23] If this is the case, as recent experiments seem to confirm, [27] then  $H_{c2}^{max}/H_{c2}^{min} = (\langle v_{ab}^2 \rangle / \langle v_c^2 \rangle)^{1/2}$ , assuming that the gap over the cylinder is essentially constant. Using the anisotropic Fermi velocities for the 2-D cylinder [23] we find that this ratio to be  $\sim \sqrt{40}$  which is in excellent agreement with the measured value of  $\gamma$  at low temperatures. A fuller and more detailed presentation of the temperature dependence of anisotropies in MgB<sub>2</sub> will be presented by Kogan *et al.*, as well as others, later

in this volume.

## 5 Critical current density

The  $M(H)$  isotherms that were used to determine  $H_{irr}(T)$  as well as  $H_c(T)$  also yielded information about the critical current density,  $J_c$ . Figure 8 presents  $J_c(H)$  for a variety of representative temperatures. The higher values of  $J_c(H, T)$  were inferred from magnetization data using the Bean model [4,12,28] and the lower values of  $J_c$  were directly measured via  $V(I)$  measurements. [4] For comparison  $J_c(H)$  data for  $\text{Nb}_3\text{Sn}$  are also shown for  $T = 4.2$  K. [29]

Several points are worth noting. First of all, even though these  $J_c$  values are lower than those for  $\text{Nb}_3\text{Sn}$  at 4-5 K, the  $J_c$  values are not all that small, especially when you consider that the sample was high purity  $\text{MgB}_2$ . In addition, at 20 K  $\text{Nb}_3\text{Sn}$  is in the normal state (i.e.  $J_c = 0$ ) whereas the  $J_c$  values for  $\text{MgB}_2$  are still sizable for low to intermediate fields. Secondly,  $J_c(H, T)$  is an extrinsic property that can be increased dramatically by judicious choices of impurities and defects to act as pinning sites. Over the past year  $J_c$  values in wire segments have increased by approximately an order of magnitude. Recent work by Finnemore *et al.* (see later in this volume) on Ti and C doped wires has shown that the low temperature, low field value of  $J_c$  can be increased to mid-  $10^6$  A/cm<sup>2</sup>. Comparable values have been found for thin film samples. [19]. Hopefully further increases in  $J_c$ , not only for low fields, but also for higher fields will continue over the next few years.

## 6 Summary

$\text{MgB}_2$  is a poster child for two very different and important observations about solid state physics. First, the field of solid state physics has come a fantastically long way given that the basic physical properties of  $\text{MgB}_2$ , as well as our theoretical understanding of them, were well delineated within less than a year of its rediscovery. This is a remarkable fact and should not be given short shrift. Secondly, superconductivity in this simple binary compound lay undiscovered until the new millennium, despite extensive searches over the past 80 years, and although superconductivity in this material is now well understood, it was not predicted *a priori*. It is vital to experimentally search for (i) new materials and (ii) new properties / groundstates in old ones. The continued search for new materials and new properties in binary, ternary, quaternary, and even more complex compounds is one of the most important engines driving this field of science.

We gratefully acknowledge useful interactions with A. H. Lacerda, M-H. Jung, N. Anderson, G. Lapertot, R. Ribiero, C. Petrovic, J. E. Ostenson, V. G. Kogan and V. P. Antropov. We also thank the U.S. D.O.E. Office of Basic Energy Sciences for the flexibility in funding that allowed us to chase after this wonder material. Ames Laboratory is operated for the U.S. Department of Energy by Iowa State University under contract No. W-7405-ENG-82. The work was supported by the Director of Energy Research, Office of Basic Energy Sciences, U. S. Department of Energy.

## References

- [1] J. Nagamatsu, N. Nakagawa, T. Muranaka, Y. Zenitani, and J. Akimitsu, *Nature* **410** (2001) 63.
- [2] S. L. Bud'ko, G. Lapertot, C. Petrovic, C. E. Cunningham, N. Anderson, P. C. Canfield, *Phys. Rev. Lett.*, **86** (2001) 1877.
- [3] R. A. Ribeiro, S. L. Bud'ko, C. Petrovic, P. C. Canfield, Los Alamos National Laboratory, Preprint Archive, Condensed Matter (2002), arXiv:cond-mat/0204510 1-16.
- [4] P. C. Canfield, D. K. Finnemore, S. L. Bud'ko, J. E. Ostenson, G. Lapertot, C. E. Cunningham, C. Petrovic, *Phys. Rev. Lett.*, **86** (2001) 2423.
- [5] S. R. Shinde, S. B. Ogale, R. L. Greene, T. Venkatesan, P. C. Canfield, S. L. Bud'ko, G. Lapertot, C. Petrovic, *Appl. Phys. Lett.*, **79** (2001) 227.
- [6] Douglas K. Finnemore; Paul C. Canfield, Sergey L. Bud'ko, Jerome E. Ostenson, Cedimir Petrovic, Charles E. Cunningham, Gerard Lapertot, U.S. Pat. Appl. Publ. (2002), International publication number WO 02/064859.
- [7] S. L. Bud'ko, C. Petrovic, G. Lapertot, C. E. Cunningham, P. C. Canfield, M. Jung, A. H. Lacerda, *Phys. Rev. B*, **63** (2001) 220503.
- [8] D. G. Hinks, H. Claus, J. D. Jorgensen, *Nature (London, UK)*, **411** (2001) 457.
- [9] T. Yildirim, O. Gulseren, J. W. Lynn, C. M. Brown, T. J. Udovic, Q. Huang, N. Rogado, K. A. Regan, M. A. Hayward, J. S. Slusky, T. He, M. K. Haas, P. Khalifah, K. Inumaru, R. J. Cava, *Phys. Rev. Lett.*, **87** (2001) 037001.
- [10] H. J. Choi, D. Roundy, H. Sun, M. L. Cohen, S. G. Louie, *Phys. Rev. B*, **66** (2002), 020513.
- [11] H. J. Choi, D. Roundy, H. Sun, M. L. Cohen, S. G. Louie, *Nature (London, UK)*, **418** (2002) 758.
- [12] D. K. Finnemore, J. E. Ostenson, S. L. Bud'ko, G. Lapertot, P. C. Canfield, *Phys. Rev. Lett.* **86** (2001) 2420.

- [13] C. U. Jung, M. S. Park, W. N. Kang, M. S. Kim, S. Y. Lee, S. I. Lee, *Physica C*, **353** (2001) 162.
- [14] C. U. Jung, H. J. Kim, M. S. Park, M. S. Kim, J. Y. Kim, Z. Du, S. I. Lee, K. H. Kim, J. B. Betts, M. Jaime, A. H. Lacerda, G. S. Boebinger, *Physica C*, **377** (2002) 21.
- [15] K. H. Kim, J. B. Betts, M. Jaime, A. H. Lacerda, G. S. Boebinger, C. U. Jung, Heon-Jun Kim, Min-Seok Park, and Sung-Ik Lee, *Phys. Rev. B* **66** (2002) 020506.
- [16] V. Braccini, L. D. Cooley, S. Patnaik, P. Manfrinetti, A. Palenzona, A. S. Siri, and D. C. Larbalestier, preprint.
- [17] Yu. Eltsev, S. Lee, K. Nakao, N. Chikumoto, S. Tajima, N. Koshizuka, M. Murakami, *Phys. Rev. B*, **65** (2002) 140501.
- [18] A. V. Sologubenko, J. Jun, S. M. Kazakov, J. Karpinski, H. R. Ott, *Phys. Rev. B*, **66** (2002) 014504.
- [19] C. B. Eom, M. K. Lee, J. H. Chol, L. J. Belenky, X. Song, L. D. Cooley, M. T. Naus, S. Patnaik, J. Jiang, M. Rikel, A. Polyanskil, A. Gurevich, X. Y. Cai, S. D. Bu, S. E. Babcock, E. E. Hellstrom, D. C. Larbalestler, N. Rogado, K. A. Regan, M. Hayward, T. He, J. S. Slusky, K. Inumaru, M. K. Haas, R. J. Cava, *Nature (London, UK)*, **411** (2001) 558.
- [20] M. H. Jung, M. Jaime, A. H. Lacerda, G. S. Boebinger, W. N. Kang, H. J. Kim, E. M. Choi, S. I. Lee, *Chem. Phys.Lett.* **343** (2001) 447.
- [21] O. F. de Lima, R. A. Ribeiro, M. A. Avila, C. A. Cardoso, A. A. Coelho, *Phys. Rev. Lett.* **86** (2001) 5974.
- [22] F. Simon, A. Janossy, T. Feher, F. Muranyi, S. Garaj, L. Forro, C. Petrovic, S. L. Bud'ko, G. Lapertot, V G. Kogan, P. C. Canfield, *Phys. Rev. Lett.* **87** (2001) 047002.
- [23] S. L. Bud'ko, V. G. Kogan, P. C. Canfield, *Phys. Rev. B*, **64** (2001) 180506.
- [24] S. L. Bud'ko and P. C. Canfield, *Phys. Rev.B*, **65** (2002) 212501.
- [25] M. Angst, R. Puzniak, A. Wisniewski, J. Jun, S. M. Kazakov, J. Karpinski, J. Roos, H. Keller, *Phys. Rev. Lett.* **88** (2002) 167004.
- [26] L. Lyard, P. Samuely, P. Szabo, C. Marcenat, T. Klein, K. H. P. Kim, C. U. Jung, H. S. Lee, B. Kang, S. Choi, S. I. Lee, L. Paulius, J. Marcus, S. Blanchard, A. G. M. Jansen, U. Welp, W. K. Kwok, Los Alamos National Laboratory, Preprint Archive, *Condensed Matter* (2002), 1-4, arXiv:cond-mat/0206231.
- [27] P. Samuely, presentation at T<sup>2</sup>PAM workshop, University of Hiroshima, August 2002.
- [28] C. P. Bean, *Phys. Rev. Lett.*, **8** (1962) 250.
- [29] Y. B. Kim and M. J. Stevens, *Superconductivity*, edited by R. D. Parks (Marcel Dekker, Inc., New York, 1969), p. 1149.



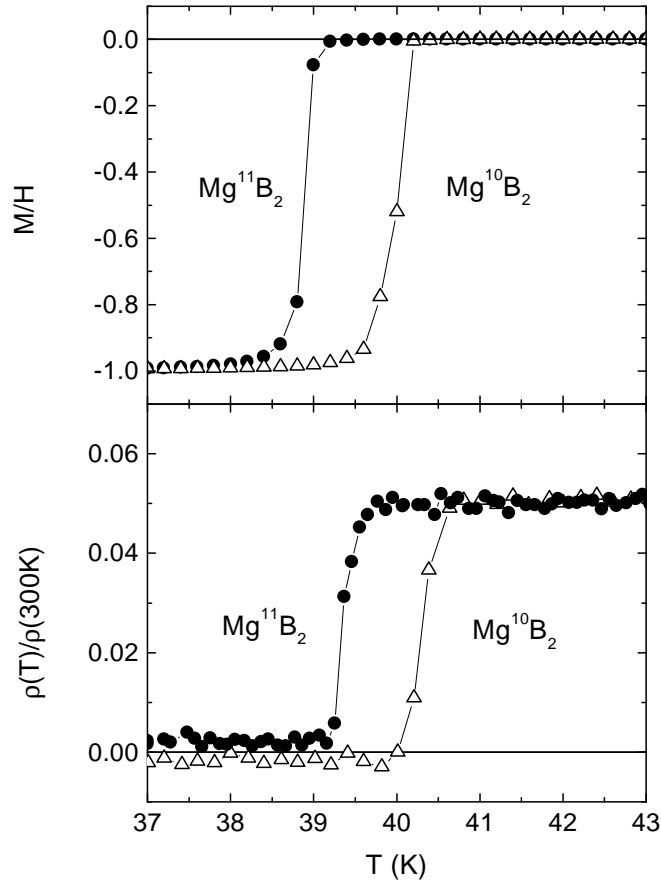


Fig. 1. Isotope shift as seen in: (upper panel) magnetization and (lower panel) resistance.

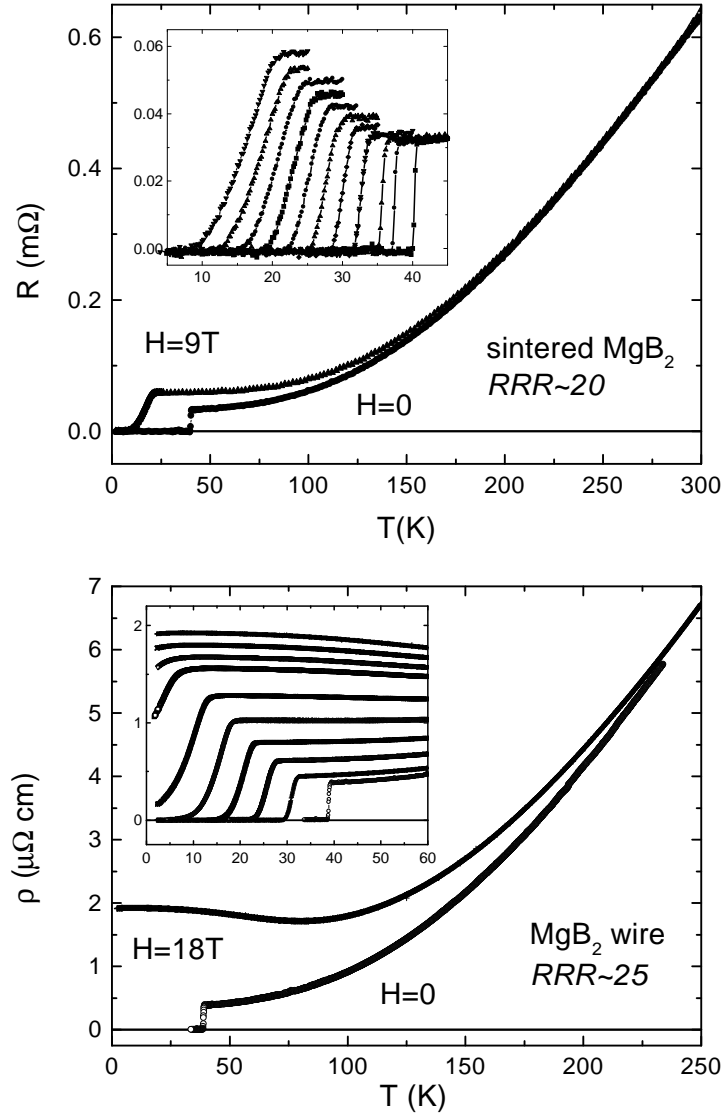


Fig. 2. Temperature dependence of electrical transport of  $MgB_2$  at given applied magnetic fields: (upper panel) resistance of sintered pellet in zero and 9 T applied field with inset showing low temperature data for applied fields of 0, 0.5, 1, 2, 3, 4, 5, 6, 7, 8, and 9 T and (lower panel) resistivity of a dense wire segment in zero and 18 T applied field with inset showing low temperature data for applied fields of 0, 2.5, 5, 7.5, 10, 12.5, 15, 16, 17, and 18 T.

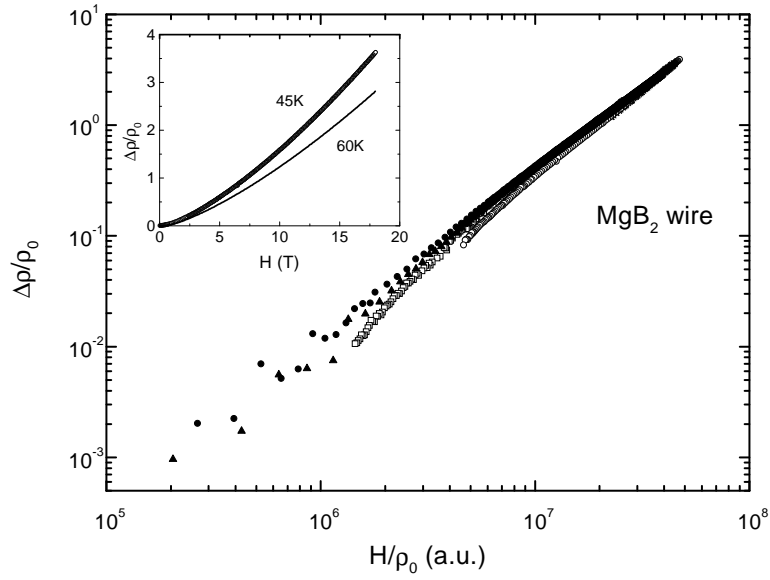


Fig. 3. Kohler's plot for  $\text{MgB}_2$  wire sample: open symbols from temperature dependent resistivity; filled symbols from field dependent resistivity taken at 45 and 60 K as shown in the inset.  $\rho_0$  is the zero field resistivity,  $\rho(T, 0)$ , and  $\Delta\rho = \rho(T, H) - \rho(T, 0)$ .

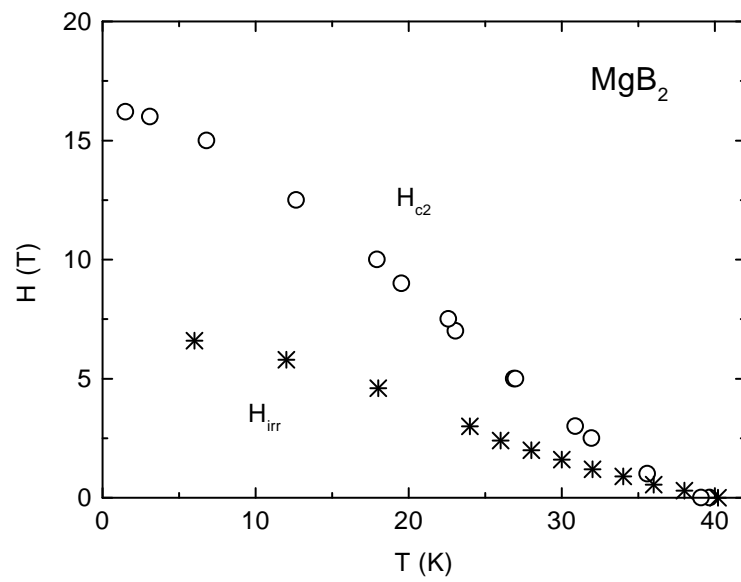


Fig. 4. Temperature dependence of  $H_{c2}$  (open circles) and  $H_{irr}$  (stars).

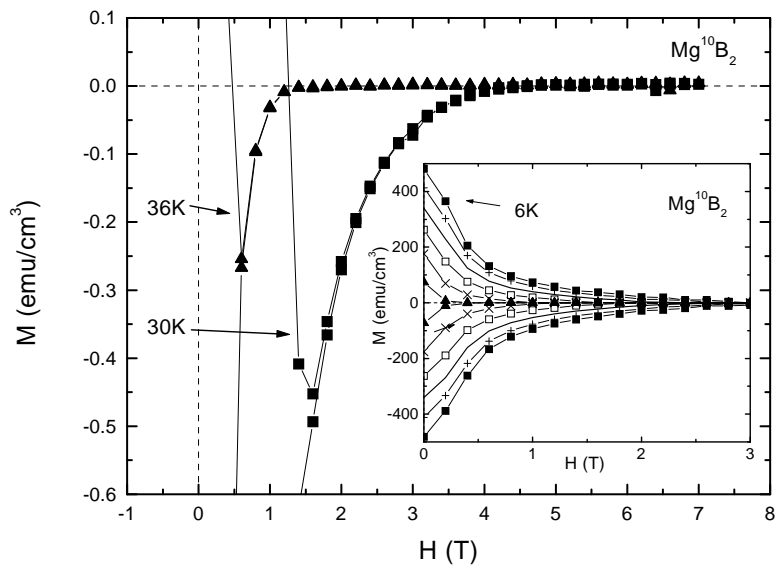


Fig. 5. Expanded view of magnetization vs. field to show the reversible range as well as  $H_{irr}$ . The inset shows the full range of magnetization data up to 3 T at temperature intervals of 6 K.

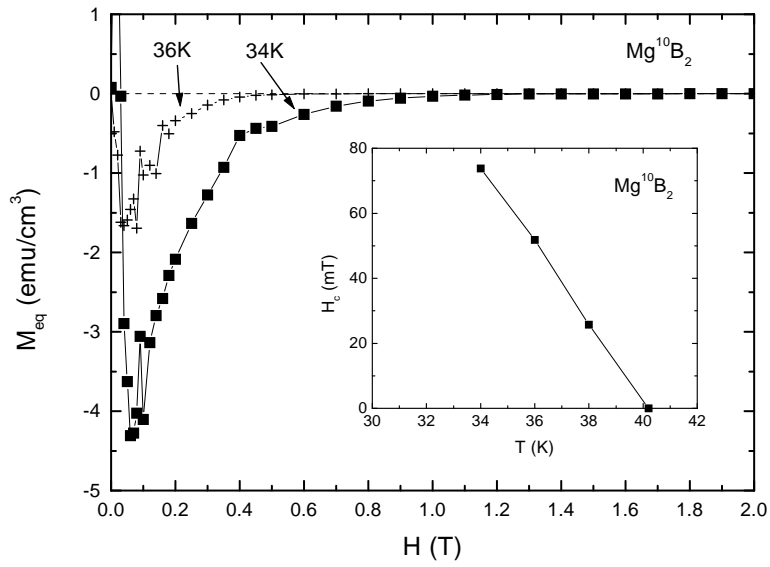


Fig. 6. Equilibrium magnetization as a function of applied field (as described in text). Inset: Thermodynamic critical field  $H_c(T)$  for  $T$  close to  $T_c$ .

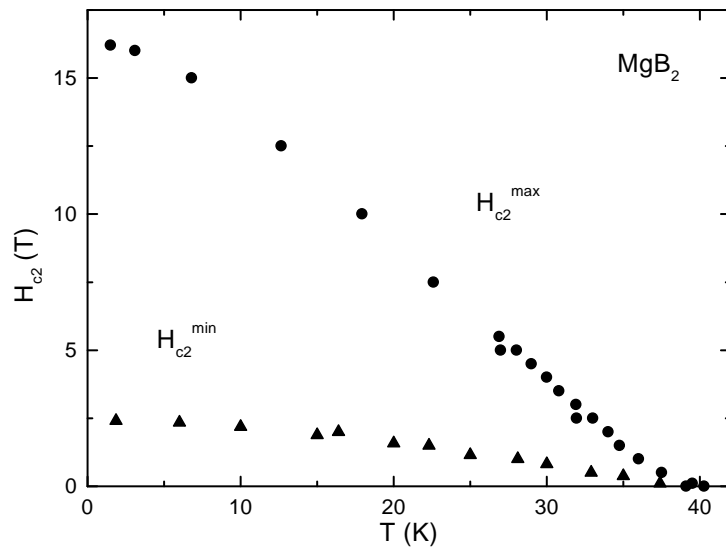


Fig. 7. Anisotropic  $H_{c2}(T)$  inferred from measurements on polycrystalline samples. (As described in references [23] and [24].)  $H_{c2}^{min}$  is the upper critical field for  $H$  parallel to the crystallographic  $c$ -axis and  $H_{c2}^{max}$  is the upper critical field for  $H$  perpendicular to the  $c$ -axis.

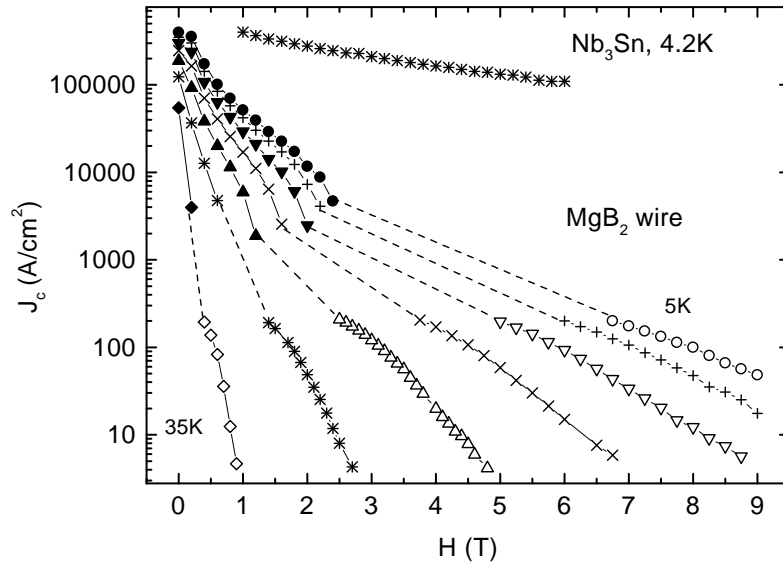


Fig. 8. Superconducting critical current density,  $J_c$ , as a function of applied field every 5 K in the 5 - 35 K range. Lower current density values, open symbols, were directly determined via  $V(I)$  measurements. Higher current density values, filled symbols, were determined via a Bean-model analysis of  $M(H)$  loops.  $J_c(H)$  data for  $\text{Nb}_3\text{Sn}$  taken at 4.2 K are shown for comparison.